Available online at www.sciencedirect.com
SCIENCE DIRECT®
Journal of Nuclear Materials 329–333 (2004) 382–386
journal of nuclear materials
www.elsevier.com/locate/jnucmat

The development and stability of Y–Ti–O nanoclusters in mechanically alloyed Fe–Cr based ferritic alloys

M.J. Alinger [a,*], G.R. Odette [a], D.T. Hoelzer [b]

[a] Department of Materials, University of California, Santa Barbara, CA 93106-5070, USA
[b] Oak Ridge National Laboratory, Oak Ridge, TN 37831-6136, USA

Abstract

Ferritic alloys containing a high density of nanoscale clusters of Y–Ti–O exhibit superior creep strength and potential for high resistance to radiation damage. Small angle neutron scattering (SANS) was used to characterize the sequence-of-events and the necessary ingredients for the formation of nanoclusters (NCs) during processing, as well as their thermal stability during high temperature aging. Mechanical alloying (MA) dissolves Y_2O_3 in the master alloy Fe–Cr–W powders. A large population of 1–2 nm NCs precipitate during subsequent high temperature consolidation. The NC sizes increase and their volume fractions and number densities decrease with increasing the consolidation temperature. Both Ti and Y are necessary for NC formation at higher temperatures. The NCs in MA957 are stable during aging at 1150 °C for times up to 243 h, but systematically coarsen at 1200 °C. The NCs coarsen rapidly and become unstable at higher aging temperatures. Variations in the alloy hardness are consistent with differences in the NC sizes and number densities.

1. Introduction

A promising approach to achieving high creep strength, radiation damage resistant alloys is to create a very high density of fine-scale features that act as dislocation obstacles, serve as the dominant nucleation site for small helium bubbles and promote vacancy–interstitial recombination. A high density of coherent, nm-scale Y–O–Ti nanoclusters (NCs) are produced by mechanical alloying (MA) Fe–Cr–Ti powders with Y_2O_3 followed by hot consolidation [1–5]. However, the detailed character of the NCs, the sequence-of-events and necessary ingredients in their formation, their stability during long-term high temperature irradiation service, and their effect on mechanical properties are not well understood. Such understanding is necessary to develop optimized properties and less costly processing paths.

Thus we seek to develop a basic understanding of the mechanisms that control the NC evolutions during processing and service, and to characterize their corresponding relations to mechanical properties. The NCs were characterized by small angle neutron scattering (SANS) and the results were compared to Vickers microhardness measurements. A transmission electron microscopy (TEM) study of a subset of alloy conditions in this paper is described in a companion paper [6].

2. Experiment

The alloy-condition codes, compositions, consolidation processes, and temperatures of the powders and alloys characterized in this study are presented in Table 1. Gas atomized master alloy powders contained ≈14-wt.% Cr, 0 and 0.4-wt.% Ti and 0 and 3-wt.%W were MA with and without 0.25-wt.% Y_2O_3 by SPEX ball milling in argon for 8 h. The milled powders were then

* Corresponding author. Tel.: +1-805 893 3212; fax: +1-805 893 8651.
E-mail address: alinger@engineering.ucsb.edu (M.J. Alinger).

0022-3115/$ - see front matter © 2004 Elsevier B.V. All rights reserved.
doi:10.1016/j.jnucmat.2004.04.042

Table 1
Alloy IDs, chemical compositions and the consolidation processes, and temperatures

Alloy ID	Alloy Element (wt.%)						Consolidation	
	Cr	Al	Ti	Mo	W	Y_2O_3	Process	Temperature (°C)
MA957	14	–	1	0.3	–	0.3	Hot ext.	1150
J12YWT	13	–	0.4	–	3	0.25	Hot ext.	1150
PM2000	20	5.5	0.5	–	–	0.5	Hot ext.	1150
U14Y	14	–	–	–	–	0.25	HIP	850, 1000, 1150
U14YT	14	–	0.4	–	–	0.25	HIP	850, 1000, 1150
U14YW	14	–	–	–	3	0.25	HIP	850, 1000, 1150
U14YWT	14	–	0.4	–	3	0.25	HIP	850, 1000, 1150
U14WT	14	–	0.4	–	3	–	HIP	850, 1000, 1150

consolidated by hot isostatic pressing (HIPing) at 200 MPa for 3 h at 850, 1000, and 1150 °C. Milled and unmilled powders were also annealed at these conditions. *Single variable* measurements were carried out by fabricating powders and consolidated alloys that served as baseline controls for a specified composition or processing variable. Thus, un-milled, milled, milled-annealed powders, and consolidated alloys established the effects of the sequence of processing steps. Likewise, for example, 14Cr–0.25Y_2O_3–3W powders and consolidated alloys served as the baseline controls for alloys with 14Cr–0.25Y_2O_3–0.4Ti–3W to evaluate the effect of Ti.

Measurements were carried out with a $\lambda = 0.5$ nm neutron beam on the 8 m SANS instrument (NG1) at the National Institute of Standards and Technology with a maximum scattering vector, $q \approx 3.0$ nm^{-1}. A strong ≈1.7 T magnetic field permitted measuring both nuclear, $d\Sigma/d\Omega(q)_n$, and magnetic, $d\Sigma/d\Omega(q)_m$, neutron scattering cross-sections, where

$$\frac{d\Sigma}{d\Omega}(q,\phi) = \frac{d\Sigma}{d\Omega}(q)_n + \sin^2\phi\,\frac{d\Sigma}{d\Omega}(q)_m. \quad (1)$$

Here ϕ is the angle with respect to magnetic field direction. Subtraction of parasitic counts and normalization of the sample counts, transmissions and masses to a water standard were carried out to measure the absolute $d\Sigma/d\Omega(q,\phi)$ that were averaged over specified detector q and ϕ ranges, typically at $\phi = 0 \pm 30$, 45 ± 15, and 80 ± 10, and used to evaluate the magnetic-to-nuclear scattering ratio (M/N).

The scattering cross-sections for the features associated with the variable of interest, $d\Sigma/d\Omega_f$, were determined by subtracting the control cross-section (see Ref. [7] for a detailed description of the SANS data reduction and analysis procedures). For example, subtracting the $d\Sigma/d\Omega$ for U14WT from that for U14YWT was used to assess the effect of Y_2O_3. The $d\Sigma/d\Omega(q,\phi)$ specify the average size ($\langle r\rangle$), size distribution ($\Delta r/r$), volume fraction (f), and number density (N) of scattering features. For features with a specified size (r)

$$d\Sigma/d\Omega(q) = NV^2(\rho_f - \rho_m)^2 S(qr). \quad (2)$$

Here ρ_f and ρ_m are the feature and matrix coherent scattering length densities and $S(qr)$ is a form factor that depends on the features shape and size [8]. We determined $\langle r\rangle$, f, and N by fitting computed $d\Sigma/d\Omega(q)_m$ curves to the $d\Sigma/d\Omega(q)$ data assuming a log-normal distribution, parameterized by mode radius, r_m, $\Delta r/r$, and $d\Sigma/d\Omega(0)_m$ [7]. However, measuring f and N requires *knowledge* of the ρ_f and ρ_m. Assuming the features are primarily Y, Ti, and O, $\rho_f \approx 0$ and the ρ_m accounted for Cr and other solutes.

The $\langle r\rangle$, N, f, and M/N were measured for MA957 thermally aged in a gettered argon atmosphere in 50 °C temperature (T_a) increments from 1150 to 1400 °C for various times (t_a) from 1 to 243 h (depending on T_a). However, good qualitative insight on the effects of composition and processing variables on the UCSB powders and the as-processed alloys can be simply obtained by comparing the $d\Sigma/d\Omega(\phi = 45 \pm 15)$ versus q^2 curves. A minimum of seven indents at a 1000 g load was used to measure the Vicker's microhardness, H_v (kg/mm^2).

3. Results and analysis

The sequence-of-events in the formation of NCs is revealed in Fig. 1. The $d\Sigma/d\Omega$ versus q^2 plots for the milled U14WT (filled circles) and U14YWT (filled squares) powders are very similar, and have a small slope in the range of $q^2 > 2$ nm^{-2}, indicating that NC features are not present in either case. The slightly higher high q scattering in the U14YWT is indicative of the presence of additional solutes or very small solute clusters. However, HIPing the U14YWT at 850 °C (filled diamonds) results in the precipitation of a high number density NCs, indicated by the large bulge in the $d\Sigma/d\Omega$ curve for q^2 between ≈1 and 6 nm^{-2}. The corresponding $d\Sigma/d\Omega$ for U14WT, without Y_2O_3, HIPed at 850 °C (open circles) is much smaller in this q-range.

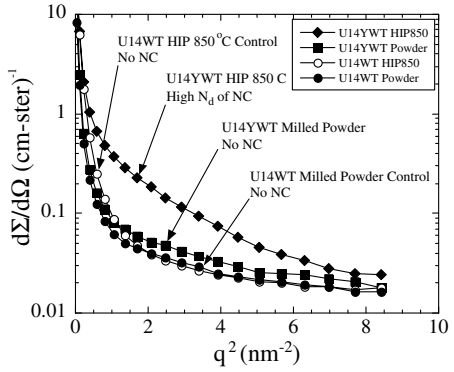

Fig. 1. SANS curves for U14YWT showing that mechanical alloying dissolves the Y_2O_3 and that the NCs form during HIP consolidation.

Fig. 2 shows the effect of HIPing (filled symbols) and powder annealing (open symbols) temperatures of 850 (squares), 1000 (diamonds), and 1150 °C (triangles) on U14YWT along with U14WT controls (small symbols). The decreases in the magnitude and increases in the slope of the $d\Sigma/d\Omega$ versus q^2 curves indicate that the $\langle r\rangle$ increases and the N and f decrease with increasing HIPing and powder annealing temperature. Notably, the scattering in the consolidated alloys and annealed powders is very similar. The powder annealed at 700 °C (upside down triangles) has the highest scattering and lowest slope, hence, the smallest $\langle r\rangle$; however, a quantitative analysis shows that the f and N are slightly smaller in this case compared to the powders annealed at 850 °C.

Fig. 3 shows the effects of alloy composition on the formation of NCs in alloys HIPed at 1150 °C. The U14YW (diamonds) and U14Y (squares) alloys without Ti do not contain NCs. However, a high density of

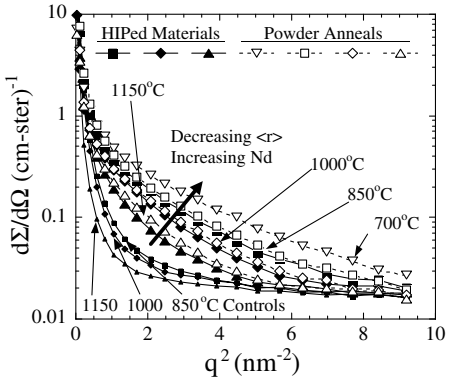

Fig. 2. The effect of HIP consolidation (closed symbols) and powder annealing (open symbols) temperatures on NC formation in U14YWT.

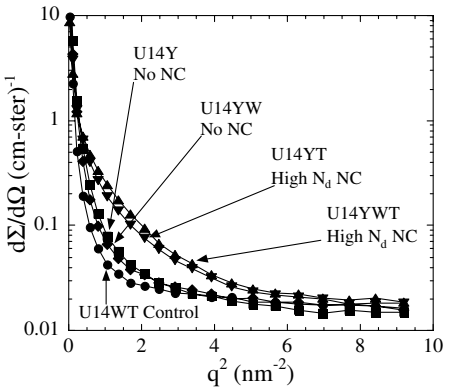

Fig. 3. The effect Ti on NC formation for HIPing at 1150 °C.

similar NCs form in both the U14YWT (upside down triangles) and U14YT (triangles) alloys with Ti. The general trends are similar at lower HIPing temperatures (not shown), but the importance of Ti is weaker in this case, and NCs are observed in U14YW and U14Y in alloys HIPed at 850 °C.

Fig. 4 shows that the NCs in U14YWT HIPed at 1150 °C (circles) are very similar to those in MA957 (squares) and 12YWT (diamonds). However, the PM2000 (triangles) alloy does not contain NCs. Note, the larger $d\Sigma/d\Omega$ at high q in this case is due to the higher Cr content of this alloy.

We summarize only the most salient results of the quantitative analysis of the thermally aged MA957. Fig. 5 shows that N decreases with increasing T_a, accompanied by increases in $\langle r\rangle$ and decreases in f (not shown). Aging at the processing temperature of 1150 °C has little effect, while aging at 1200 °C produces a systematic coarsening and a decrease in f by a factor of $\approx$0.7 at a constant M/N. The N and $\langle r(t_a)\rangle^3 - \langle r(0)\rangle^3$ approximately scale with t_a^{-1} and t_a, respectively, in this case,

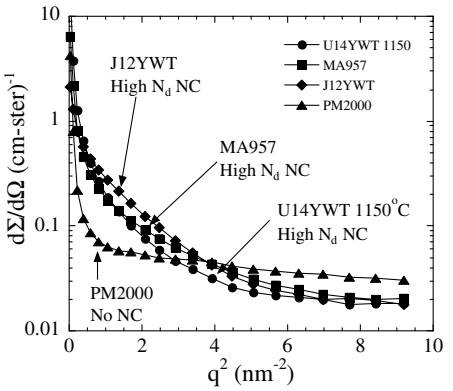

Fig. 4. Comparison of NC scattering in U14YWT, MA957, J12YWT, and PM2000.

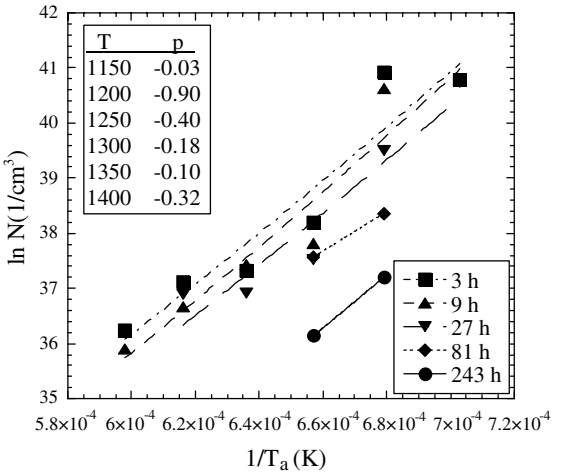

Fig. 5. The $\ln N$ as a function of $1/T_a$ for various t_a in the aged MA957. The inset table shows the fit parameters, p, for the relation $N = C(T)t_a^p$.

consistent with a classical bulk diffusion controlled coarsening. In contrast, aging at 1250 °C produces a rapid drop in N at 3 h. While the NCs are significantly larger in this case, they have a similar f and M/N. Subsequent NC growth occurs at longer t_a occurs at an apparently fluctuating f and constant M/N. The decrease in N and increase $\langle r(t_a)\rangle^3 - \langle r(0)\rangle^3$ at 1250 °C scale with $\approx t_a^{-0.3}$. At still higher T_a the N continues decrease with large jumps at 3 h, again followed by non-classical coarsening scaling with t_a^{-p}, where $p \ll 1$ as shown in Fig. 5. Both f, and particularly M/N, are larger at the highest t_a of 1350 and 1400 °C. Additional data and analysis is needed to understand this complex behavior. However, in summary, the NCs classically coarsen at 1200 °C, undergo a rapid instability at 1250 °C and experience another transition at and above 1350 °C.

These complex results suggest that there is not one single mechanism controlling the evolution of NCs under high temperature aging. Analysis of the N and $\langle r(t_a)\rangle^3 - \langle r(0)\rangle^3$ data yields effective activation energies Q_e of ≈400 and 300 ± 20 kJ/mole, respectively. The value of 300 kJ/mole is reasonably consistent with typical values for solute and self-diffusion in iron [9]. Note a much higher, and non-physical, Q_e is indicated by the relative stability of the NCs between 1150 and 1200 °C. If we assume that diffusion controlled kinetics the $Q_e \approx 300$–400 kJ/mole are applicable to lower aging temperatures, pertinent to service conditions, we can estimate the corresponding coarsening rates. Assuming a Q_e of 300 kJ/mole the NC stability at 1150 °C after 243 h would correspond to $t_a \approx 10^5$ h at 800 °C. The modest but significant coarsening at 9 h and 1200 °C would correspond to t_a of 8.3×10^4 to 1.75×10^6 h at $T_a = 800$ °C for Q_e of 300 and 400 kJ/mole, respectively. This suggests that the NCs will be either stable or very stable at expected service temperatures. However, long-time aging studies of aging below the final processing temperature are needed to confirm this conclusion.

Fig. 6 plots the H_v, including some alloy conditions not explicitly discussed here versus $f^{1/2}/\langle r\rangle$. The data fall into two hardening rate categories of $\Delta H_v/\Delta[f^{1/2}/\langle r\rangle]$, as indicated by the slopes of the two least square fit lines. The higher hardening rate is generally associated with the alloys containing Y–Ti–O NCs HIPed at 850 and 1000 °C and 12YWT. The alloys with a lower hardening rate include the MA957 in both the as-processed and aged conditions, other powders HIPed at 1150 °C with and without Ti, as well as powders with Ti that were attritor milled with Y_2O_3 at Oak Ridge National Laboratory. Presumably, most of the hardening is due to NCs. The increase in the yield stress, $\Delta\sigma_y$, due to dispersed barrier obstacles to dislocation slip is given by [10]

$$\Delta\sigma_y \approx 3\alpha Gb/\lambda \approx 1.68\alpha Gbf^{1/2}/\langle r\rangle. \quad (3)$$

Here the 3 is the Taylor factor, α is the obstacle strength parameter (<0.8), G and b are the Fe shear modulus (≈80 GPa) and Burger's vector (0.25 nm), respectively, and λ is the obstacle spacing on a slip plane, where $1/\lambda = 0.56f^{1/2}/\langle r\rangle$ [10]. Assuming $\Delta\sigma_y$ (MPa) $\approx 3\Delta H_v$ (kg/mm^2) the slopes of the lines in Fig. 6 can be used to estimate effective values of $\alpha \approx 0.33$ and 0.5. However, a significant Hall–Petch type contribution from the small grain-subgrain size is also expected. Since the grain/subgrain size is also influenced by the processing conditions and boundary pinning by the NCs themselves, it is difficult to separate the two contributions to $\Delta\sigma_y$.

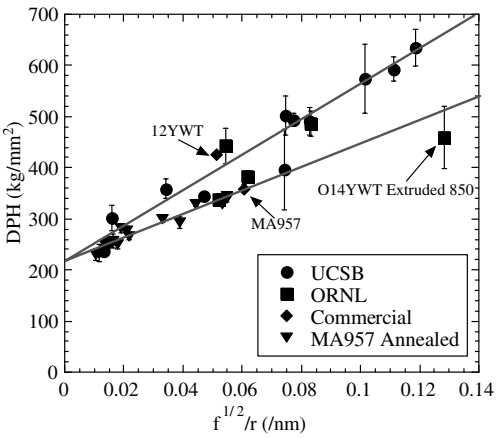

Fig. 6. The H_v as a function $f^{1/2}/r$ showing two hardening regimes.

4. Conclusions

The results of this study can be summarized as follows:

- The Y_2O_3 dissolves during mechanical alloying.
- Y–Ti–O enriched NCs precipitate during high temperature consolidation.
- Increasing consolidation temperature results in larger NC sizes and smaller number densities and volume fractions.
- The NCs that form in annealed MA powders are nearly identical to those in HIP consolidated alloys.
- Both Y and Ti are required for the formation of high number density NCs at higher HIPing temperatures.
- The NCs in U14YWT HIP consolidated at 1150 °C are similar to those found in MA957 and J12YWT that are extruded at the same temperature.
- The NCs in MA957 are expected to be thermally stable at service temperatures around 800 °C.
- There is an excellent correlation between microhardness and the size and volume fraction of the NCs or their spacing on a slip plane.

Acknowledgements

The authors gratefully acknowledge Doug Klingensmith (UCSB) for his contributions to the SANS experiments and Professor Brian Wirth (UC Berkeley) for his help in analysis of the SANS data. We acknowledge the support of the National Institute of Standards and Technology, US Department of Commerce, in providing facilities used in this work. This research was supported by DOE Office of Fusion Energy Science (Grant # DE-FG03-94ER54275) and the INERI DOE Office of Nuclear Energy through a subcontract with ORNL (Grant # 400014112).

References

[1] J.S. Benjamin, Metall. Trans. 1 (10) (1970) 2943.
[2] S. Ukai, T. Nishida, H. Okada, J. Nuc. Sci. Technol. 34 (3) (1997) 256.
[3] S. Ukai, T. Nishida, T. Okuda, T. Yoshitake, J. Nucl. Mater. 258–263 (1998) 1745.
[4] T. Okuda, M. Fujiwara, J. Mater. Sci. 14 (1995) 1600.
[5] M.K. Miller, E.A. Kenik, K.F. Russell, L. Heatherly, D.T. Hoelzer, P.J. Maziasz, Mater. Sci. Eng. A A353 (2003) 140.
[6] H. Kishimoto, M.J. Alinger, G.R. Odette, T. Yamamoto, J. Nucl. Mater., this issue.
[7] E. Mader, PhD thesis, University of California, Santa Barbara, 1995.
[8] A.-J. Dianoux, G. Lander (Eds.), ILL Neutron Data Booklet, Institut Laue-Langevin, 2001.
[9] J. Kucera, K. Stransky, Mater. Sci. Eng. 52 (1982) 1.
[10] J.W. Martin, Micromechanisms in Particle-Hardened Alloys, Cambridge University, 1980.